Progress In Electromagnetics Research, Vol. 132, 49–69, 2012

DESIGN OF RF ENERGY HARVESTING SYSTEM FOR ENERGIZING LOW POWER DEVICES

N. M. Din[1], C. K. Chakrabarty[1], A. Bin Ismail[1], K. K. A. Devi[2, *], and W.-Y. Chen[2]

[1]Department of Electronics and Communication Engineering, Universiti Tenaga Nasional, Putrajaya Campus, Kajang-43000, Malaysia

[2]Department of Electrical and Electronic Engineering, INTI International University, Nilai-71800, Malaysia

Abstract—Electromagnetic energy harvesting holds a promising future for energizing low power electronic devices in wireless communication circuits. This article presents an RF energy harvesting system that can harvest energy from the ambient surroundings at the downlink radio frequency range of GSM-900 band. The harvesting system is aimed to provide an alternative source of energy for energizing low power devices. The system design consists of three modules: a single wideband 377 Ω E-shaped patch antenna, a pi matching network and a 7-stage voltage doubler circuit. These three modules were fabricated on a single printed circuit board. The antenna and Pi matching network have been optimized through electromagnetic simulation software, Agilent ADS 2009 environment. The uniqueness of the system lies in the partial ground plane and the alignment of induced electric field for maximum current flow in the antenna that maximizes the captured RF energy. The design and simulation of the voltage doubler circuit were performed using Multisim software. All the three modules were integrated and fabricated on a double sided FR 4 printed circuit board. The DC voltage obtained from the harvester system in the field test at an approximate distance of 50 m from GSM cell tower was 2.9 V. This voltage was enough to power the STLM20 temperature sensor.

Received 20 July 2012, Accepted 13 September 2012, Scheduled 21 September 2012

* Corresponding author: Kavuri Kasi Annapurna Devi (kavurik.adevi@newinti.edu.my).

1. INTRODUCTION

There is an active research area investigating a number of alternative ways to extract energy from the environment and convert it into electrical energy for energizing low power electronic circuits directly or store it for later use. One such energy is from radio frequency. RF Energy harvesting from the ambient will have an important role in the future microelectronic circuits. This work is being carried out by many researchers for the following reasons: i. The energy is freely available in space. ii. Complementing the low power sources used for energizing the low power electronic devices, as an application to green technology. RF energy harvesting from ambient sources have great potential to impact on the cellular phones and portable electronic devices. This concept needs an efficient antenna along with a circuit capable of converting RF signals into DC voltage, so as to replace the need for batteries.

The author in [1] designed a rectenna for 2.45 GHz using tuning procedure to energize the sensors in a remote fashion for context aware spaces, maximum distances obtained was $\leq$ 1 m in lab tests. In [2] energy is scavenged through solar and vibrational energy sources and a custom built 1.9 GHz RF direct modulated transmit beacon was developed, this represents the technological advances made in energy scavenging and ultra low power RF circuit design. A RF-DC power conversion system designed in CMOS technology at 906 MHz [3], achieved 1 V DC output at 0.3 µA for a received power of 5.5 µW (-22.6 dBm). In [4] by boosting and regulating the received power from a mobile phone using surface mount devices on a silicon chip obtained 4.0 V at 1 mA to power the sensors periodically for 10 mS. Authors in [5, 6] used resonance circuit transformation with a RF-DC Schottky-Diode charge pump for 50 Ω impedance at 900 MHz and 300 MHz respectively. They obtained a quality factor of 28 and 25 with DC output voltage of 0.3 V and 0.377 V respectively for a received power of -26 dBm (2.5 µW) and 0 dBm (1 mW). These low DC voltages are given to a Boost converter TPS61200 to power a micro system after a period of harvesting. In [7] the rectifier circuit with 50 mV input for frequency range 902–928 MHz achieved a maximum efficiency of 60%. Authors in [8] presented that power density levels' ranging from 0.1 mW/m^2 to 1.0 mW/m^2 was achieved for a spot low frequency at a distance of 25 m to 100 m from GSM-900 and GSM-1800 base stations in the WLAN environment. In [9] the authors proposed a system to charge a small battery or to run a low power sensor at frequency range of 950 MHz–960 MHz. Due to frequency hopping of signals suggested to use a DSP processor, in which main challenge was powering up the DSP processor. In [10] the RF energy harvesting system was designed

based on microstrip patch antenna at 3.25 GHz, with 100 Ω impedance, yields a return loss of 10.21 dB through simulation and used a 7-stage Schottky diode charge pump circuit that directly power a light emitting diode. The Authors in [11] developed a CMOS based Villard voltage multiplier that captured RF energy by placing it adjacent to an RF source with power ranging from −10 dBm to 5 dBm. In [12] an RF energy harvesting system was designed with a 50 Ω gap coupled micro strip antenna at 2.67 GHz and 5.8 GHz achieved a gain of 8.6 dB and 9 dB, a bandwidth of 100 MHz and 690 MHz used a CMOS 5-stage rectifier circuit obtained an output voltage of 1.04 V into 1 MΩ load at 2.67 GHz. The authors in [13] designed a square microstrip antenna with 50 Ω impedance and used a 6-stage Schottky diode voltage doubler to form an RF energy harvesting system at 900 MHz band. This work achieved an output voltage of 2.78 V and 0.87 V at a distance of 10 m and of 50 m respectively for a received power levels of 4 dBm and 5 dBm from a 900 MHz cell tower. In [14] the authors designed a broadband log periodic antenna at 674–680 MHz and used a 4-stage RF-DC conversion circuit. They obtained an output voltage of 1.5 V at 25 μA which was used to power a thermometer at 4.1 km distance from a transmitter that broadcasts 960 kW of power. In the market, power harvester modules are produced at 915 MHz from a 4 W intentional RF energy source [15]. The authors in [16] designed patch antenna and antenna array at 5.8 GHz for WLAN application achieved DC voltage of 72.5 mV and 428.3 mV using Schottky diode and LTC5535 (RF power detector) for RF-DC conversion from 16 dBm power source at a distance of 15 cm. Microstrip patch antenna has been designed to operate at 2.4 GHz ISM band to capture directed RF energy and charged a supercapacitor to power a sensor node to 3.6 V in 27 s [17].

In this article a novel RF energy harvesting system is designed with partial ground plane for energizing low power devices. The system produces DC output voltage of 2.9 V at 100 kΩ and at a distance of 50 m from GSM cell tower, used to energize a low power device. The special features of this designed system are in the impedance of the antenna, matching network, ground plane technique and frequency of operation (downlink radio frequency range of GSM-900 band) which all differs from the previous works described.

Section 2 describes the design of the RF energy harvestings system. Section 3 describes the procedure of measurements. Section 4 discusses both simulated, measured results of the modules and the system performance. And Section 5 is the conclusion.

2. RF ENERGY HARVESTING SYSTEM DESIGN

This section, deals with the design of the following modules: i. an antenna for maximizing RF signal, ii. a suitable matching network to match the complex load impedance to the antenna impedance, iii. optimization of voltage doubler stages in RF-DC conversion module.

2.1. Antenna Design [18]

The proposed antenna was an E-shaped single patch from the conventional wide band microstrip antennas. The topology of the antenna was designed on a FR4 substrate. It is a grade designation assigned to glass-reinforced epoxy laminate sheets and printed circuit boards (PCBs). This is one of the popular industry-wide standard substrate material format for electronic circuit boards. The key property of FR4 relates to the flame retardant qualities of the material. The important specifications chosen in simulation for this design are: the thickness of substrate 1.6 mm, the thickness of copper 0.035 mm, the relative permittivity 3.9, and the loss tangent 0.01. The antenna size is characterized by its length, width and height (L, W, h) and is fed by pi matching network, feed line and is followed by a partial ground plane. The antenna is designed and optimized to capture the energy from the ambient at downlink radio frequency range of GSM-

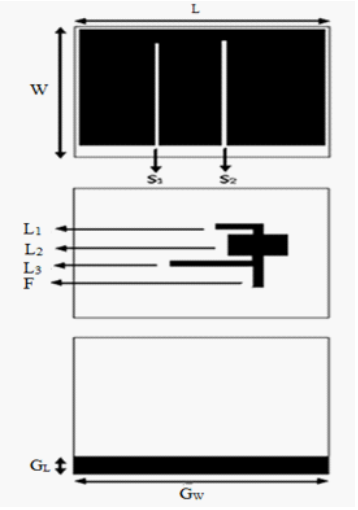

Figure 1. Configuration of E-shaped patch antenna with pi matching network and partial ground plane.

900 band. In order to expand its bandwidth, two parallel slots are incorporated into this patch. The pi matching network is designed and optimized to provide an impedance matching for the antenna $377\,\Omega$ impedance to the complex load 63-$j117\,\Omega$ impedance (input of the RF-DC convertor). The feed line is appropriately positioned at the upper leg of the E-shaped patch antenna as shown in Figure 1. The slot length, width, and position are important parameters in controlling the achievable bandwidth.

Traditionally, the property of the patch antenna is suitable for narrow bandwidth applications. The challenge here is to make the patch antenna for wideband energy harvesting environment. The antenna design required to look into the permittivity or dielectric constant of the substrate, width, length of the patch antenna and the ground plane. The permittivity of the substrate plays a major role in the overall performance of the antenna. It affects the width, the characteristic impedance, the length and therefore the resonant frequency that resulting to reduce the transmission efficiency. Using a permittivity value ε_r of 3.9, the effective dielectric constant ϵ_{reff} of the antenna is determined from the Equation (1) which was obtained from [19, 20].

For $W/h > 1$

$$\varepsilon_{reff} = \frac{\varepsilon_r + 1}{2} + \frac{\varepsilon_r - 1}{2}\left[1 + 12\frac{h}{W}\right]^{-\frac{1}{2}} \tag{1}$$

In the xy-plane due to fringing effects, the dimensions of patch along its length is extended by a distance ΔL, which is a function of the effective dielectric constant ϵ_{reff} and the width-to-height ratio (W/h).

The length (L) of the patch determines the resonant frequency and is calculated using Equations (2) and (3)

$$L = \frac{\lambda}{2} - \Delta L = \frac{1}{2f_r\sqrt{\varepsilon_{reff}}\sqrt{\mu_0\varepsilon_0}} - 2\Delta L \tag{2}$$

where

$$\Delta L = 0.412\,X\,h \times \frac{(\varepsilon_{reff} + 0.3)\left(\frac{W}{h} + 0.264\right)}{(\varepsilon_{reff} - 0.258)\left(\frac{W}{h} + 0.8\right)} \tag{3}$$

The width (W) of the patch is critical in terms of power efficiency, antenna impedance and bandwidth. It is dependent on the operating frequency and the substrate dielectric constant. The Equation (4) was used to determine the width.

$$W = \frac{1}{2f_r\sqrt{\mu_0\varepsilon_0}}\sqrt{\frac{2}{\varepsilon_r + 1}} = \frac{v_0}{2f_r}\sqrt{\frac{2}{\varepsilon_r + 1}} \tag{4}$$

Table 1. Dimensions of antenna geometry.

Basic Configuration	Patch antenna						Pi matching network						Feed line		Ground plane	
Variable	W	L	S_1		S_2		L_1		L_2		L_3					
			W	L	W	L	W	L	W	L	W	L	W	L	G_W	G_L
Dimensions (mm)	85	106	79	2	81	3	2	10	13	8	2	20	8	3	8	110

The two slots on the antenna are denoted by S_1 and S_2. The three components of the pi matching network are represented by L_1, L_2 and L_3 respectively. The feed line is denoted by F. The structure of the E shaped patch antenna and the pi matching network are printed on one side of the FR 4 substrate with the partial ground plane on the other side. The partial ground plane is denoted by G_L and G_w as shown in Figure 1. The design parameters such as dimension (length and width) of patch, slots, pi matching network, the feed line and the partial ground plane are optimized to obtain the best return loss and wide impedance bandwidth. The dimensions of the proposed antenna, pi matching network, feed line and the partial ground plane are as shown in Table 1.

2.2. Energy Conversion Module (RF-DC) [21]

The energy conversion module is a voltage doubler circuit used to convert the harvested energy from ambient radio frequency into DC voltage. The design contains stages of Villard voltage doubler circuit. The function of the energy conversion module is to convert the (RF) signals into direct-current (DC) voltage at the given frequency band to power the low power devices/circuits. The design is based on the Villard voltage doubler circuit. A 7-stage Schottky diode voltage doubler circuit is designed, modeled, simulated, fabricated and tested. Multisim was used for the modeling and simulation. Simulation and measurement were carried out for various input power levels at the specified frequency band. For an equivalent incident signal of -40 dBm, the circuit produced 3 mV across a 100 kΩ.

The voltage multiplier circuit in this design uses zero bias Schottky diode HSMS-2850 from Agilent. The attractive features of this diode are low forward voltage, low substrate leakage, very fast switching and uses the non symmetric properties of a diode that allows unidirectional flow of current under ideal condition but leads to a fabrication overhead.

Each independent stage with its dedicated voltage doubler circuit can be seen as a single battery with open circuit output voltage V_0, internal resistance R_0. With load resistance R_L, the output voltage, V_{out} is expressed as in [22].

$$V_{out} = \frac{V_0}{R_0 + R_L} R_L \tag{5}$$

When n number of these circuits are put in series and connected to a load of R_L in Equation (5) the output voltage V_{out} obtained is given by

$$V_{out} = \frac{nV_0}{nR_0 + R_L} R_L = V_0 \frac{1}{\frac{R_0}{R_L} + \frac{1}{n}} \tag{6}$$

The number of stages in the system has the greatest effect on the output voltage. The capacitors, both in the stages and at the final stage of the circuit, affect the speed of the transient response and the stability of the output signal. The number of stages is essentially directly proportional to the amount of voltage obtained at the output of the system.

2.3. Matching Network

The matching network in the geometry was designed to provide a good impedance match for complex load (RF-DC convertor) impedance 63-$j117\,\Omega$ to source (antenna) impedances $377\,\Omega$ to transform maximum power from the source to the load. The output of the pi matching network is directly connected to the input of RF-DC converter circuit. The design of pi matching network starts off with the lumped elements model where by the matching network have shunt open circuit capacitors and a series inductor. The lumped elements in the matching network are then transformed into distributed elements to obtain the initial values of length and width for each distributed component using the Equations (7) to (9). By using ADS the optimized dimensions of the distributed elements in the matching network were obtained.

$$Z_{in}^{oc} = -jZ_0 \cot \beta l = -j50 \cot \beta l \tag{7}$$

where

$$\beta = \frac{2\pi}{\lambda} \quad \text{and} \quad \lambda = \frac{\lambda_0}{\sqrt{\varepsilon_{reff}}}$$

$$Z_{cap}^{oc} = \frac{1}{j\omega C} \tag{8}$$

$$Z_{ind}^{oc} = j\omega L \tag{9}$$

3. METHODOLOGY

This section describes the methodology undertaken to design the modules of the RF energy harvesting system. Figure 2 presents the conceptual block diagram of an energy harvesting system, which comprised of antenna, band pass matching network, and energy conversion module, filter and load circuit.

3.1. Antenna Module [18]

The properties and performance of the proposed antenna have been predicted and optimized through electromagnetic simulation software in Agilent ADS 2009 environment. The method of moments (MOM) was used for analysis and the Green's vector function was chosen as the basis function to demonstrate the performance of the wide band configuration. The characteristics of the fabricated antenna have been measured using the Advantest R3767CG network analyzer.

3.1.1. Performance Study with Various Dimensions of Antenna Geometry

A performance study was conducted with various dimensions of antenna geometry. This study includes the rectangular patch plus the pi matching network to determine the best structure and dimensions for the antenna. The investigations were focussed on the effect of the ground plane towards the performance of the required parameters: Return loss better than -20 dB at resonance with an impedance match close to $50\,\Omega$, impedance bandwidth (-10 dB) better than 150 MHz and a good overall performance of antenna at the desired frequency

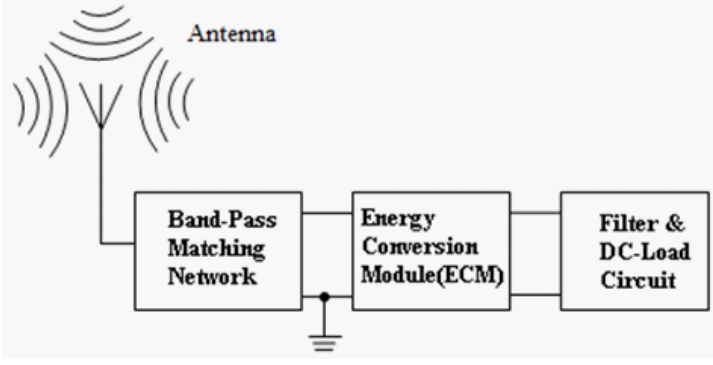

Figure 2. Conceptual block diagram for energy harvesting system.

range to satisfy the end application requirement. Parametric study was performed and the best geometry that fulfilled the requirement for the design specifications was chosen.

The pi matching network is appropriately positioned at the upper edge of the E-shaped [23] patch antenna was as shown in Figure 3. The slot length, width, and position are important parameters in controlling the achievable bandwidth and the overall performance of antenna.

The results of return loss is shown in Figure 4. It is observed that the structure is resonating at 941.7 MHz with return loss of −39.99 dB, giving an impedance bandwidth of 285 MHz (30.26%@941.7 MHz). The simulation to results of impedance is shown in Figure 5. The

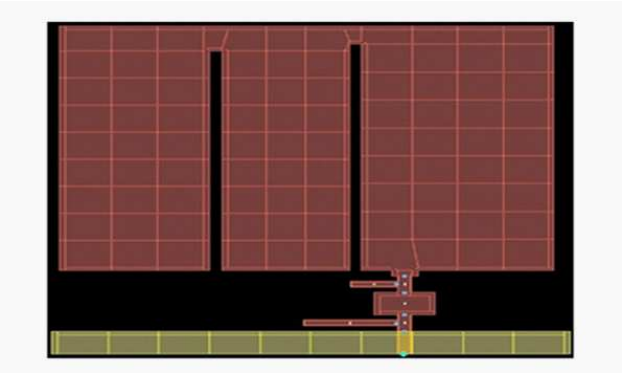

Figure 3. Screen capture of E-shaped patch antenna.

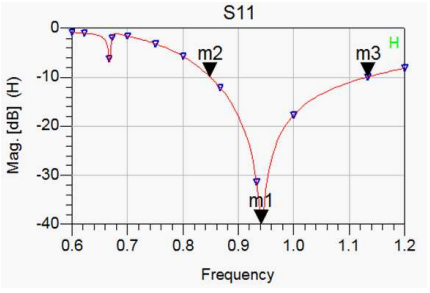

Figure 4. Simulation results of return loss.

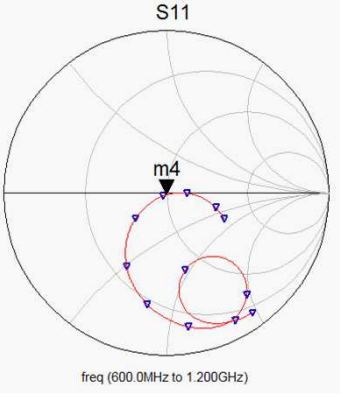

Figure 5. Simulation results of impedance on Smith chart.

real part of the impedance at the resonant frequency (m2) is 54.3 Ω, close to 50 Ω in the desired range of frequency band. The reactive part of the impedance is 0.1 Ω, almost negligible and is capative.This indicates the best impedance match from the load to the source.

A field test was conducted in the vicinity of GSM cell towers. In order to test the performance of the antenna for both uplink (890.2–914.8 MHz) and down link (935.2 MHz–959.8 MHz) radio frequency bands, the test frequencies were chosen from the spectrum analyzer to cover both the frequency bands. The start frequency was set as 890 MHz and end frequency was set at 970 MHz, which is shown in Figure 10.

3.2. RF-DC Conversion Module [21]

Modeling and simulation was carried out in Multisim software environment. The simulation and practical implementation was done with fixed RF at 945 MHz ± 100 MHz, which is close to the down link center radio frequency (947.5 MHz) of GSM-900 band. The voltage obtained at the final node (V_{DC7}) of the doubler circuit was recorded for various input power levels from −40 dBm to +5 dBm with power level interval (spacing) of 5 dBm. The input impedance 63-j117 Ω of the voltage doubler is obtained using the network analyzer. This 63-j117 Ω was tested from 900 MHz to 1000 MHz. as the antenna was designed for the down link radio frequency range of GSM-900 band.

Figure 6 shows the photograph of the assembled circuit board of 7-stage RF-DC conversion module. The design of the printed circuit board (PCB) was carried out from the DipTrace software. The PCB was manufactured on FR 4 substrate and has thickness of 1.6 mm and dielectric constant of 3.9. The dimension of PCB is 98 mm × 34 mm.

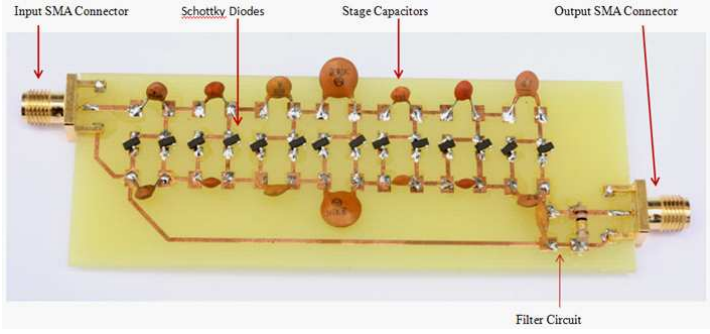

Figure 6. Photograph of assembled circuit board of 7-stage voltage doubler.

The SMA connectors are used at the input and output of PCB to carry out the measurements. The circuit consists of active and passive components. Special handling precautions have been taken to avoid Electro Static Discharge (ESD) while assembling the surface-mount zero bias Schottky diodes. Also special attention has been given to mount other components and the SMA connectors on to the PCB.

3.3. Matching Network

Figure 7 shows the schematic of pi the matching network used to transform the complex load 63-$j117\,\Omega$ impedance at the input of the voltage doubler (RF-DC conversion circuit) to the $377\,\Omega$ impedance of the antenna.

The transmission line calculator is used to obtain microstrip components in the matching network. The line calculator uses Equation (10) for the characteristic impedance Z_0.

$$\varepsilon_{eff} = \frac{\varepsilon_r + 1}{2} + \frac{\varepsilon_r - 1}{2}\left[\frac{1}{\sqrt{1 + 12\left(\frac{H}{W}\right)}} + 0.4\left(1 - \frac{W}{H}\right)^2\right] \quad \text{for} \frac{W}{H} < 1$$

$$Z_0 = \frac{60}{\sqrt{\varepsilon_{eff}}} \ln\left(\frac{8H}{W} + \frac{W}{4H}\right)\ \Omega \tag{10}$$

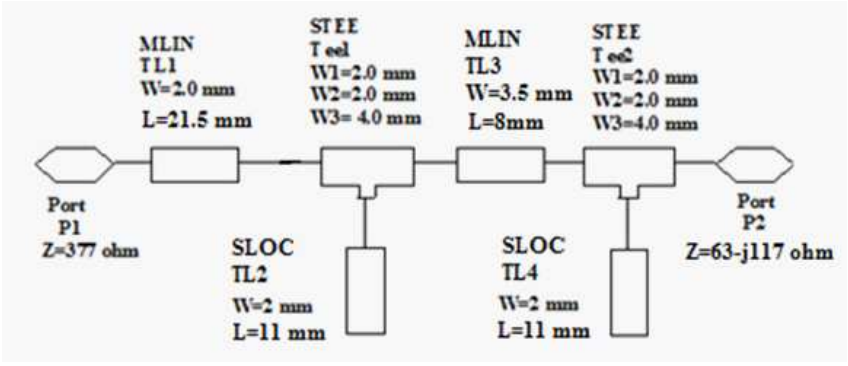

Figure 7. Schematic of pi matching network for complex load 63-$j117\,\Omega$ to $377\,\Omega$ impedance of antenna.

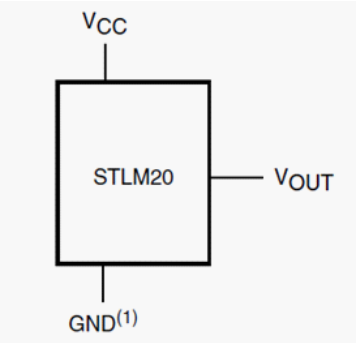

Figure 8. Logic diagram of temperature sensor.

3.4. Powering the Temperature Sensor STLM20

The logic diagram of the STLM20 is shown in Figure 8. The energy harvesting system is used to power a low power temperature sensor STLM20 to measure the ambient temperature. The STLM20 is a precision analog output temperature sensor for low current applications [24, 25], where maximizing battery life is important. The operating voltage range is 2.4 V to 5.5 V.

The analog output voltage V_0 of the sensor can be obtained using a linear transfer function given by the Equation (11) [24].

$$V_0 = \frac{-11.96\,\text{mV}}{^\circ\text{C}} \times T + 1.8663\,\text{V} \tag{11}$$

The temperature of the environment can be computed using the Equation (12) [24].

$$T = -1481.96 + \sqrt{2.1962 \times 10^6 + \frac{(1.8639 - V_0)}{3.88 \times 10^{-6}}} \tag{12}$$

4. RESULTS AND ANALYSIS

In this section, all the simulated, measured, field test results and analysis for the energy harvesting system are discussed.

4.1. Results of Antenna [18]

The return loss for both simulation and test is shown in Figure 9. From the graphs it is observed that the return losses −39.99 dB at 941.7 MHz in simulation and −35 dB at 955 MHz in test were obtained. The values of the resonant frequency and relative bandwidth for simulation and

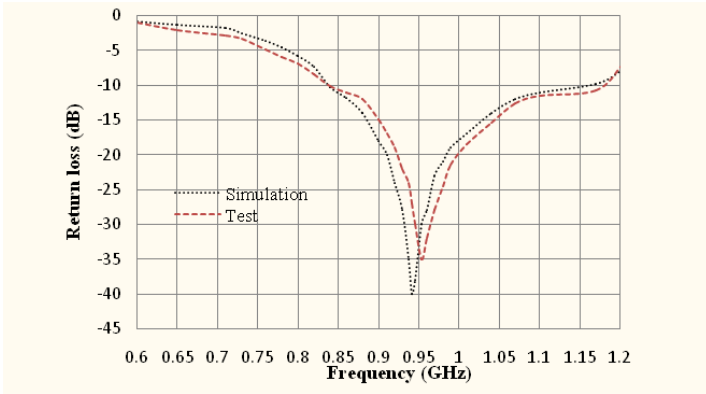

Figure 9. Results of simulation and test for return loss (dB) verses frequency (GHz).

Table 2. Results of simulation and Test for return loss.

Frequency (MHz)	Simulation	Test
At -10 dB f_l and f_h Frequency (MHz)	840 and 1170	845 and 1180
Bandwidth (MHz)	330 (35%@941.7)	335 (35.1%@955)
Return loss (S_{11})	-39.99 dB (941.7 MHz)	-35 dB (955 MHz)

test are shown in Table 2. These analyses show that the results of measured and simulated antenna performance follow the same trend with in the frequency range of the GSM-900 band.

4.2. Antenna Field Test Results

The E-shaped patch antenna designed for 377 Ω used in the RF energy harvesting system was tested in outdoor fields at 2 locations in different terrains.

Location 1: This field test of the receiving E-patch antenna was conducted at the same level from ground and at line of sight with the GSM transmitting antenna at a distance of 400 m between them. The power spectrum obtained is shown in Figure 10 and the results of performance are shown in Table 3. It is observed that the designed antenna started capturing signals from 936 MHz to 958.12 MHz which lies well within the downlink radio frequency range of GSM-900 band; beyond this frequency band the spectrum shows only the presence of noise. The peak signal of -16.64 dBm was observed at 958.12 MHz

Table 3. Field test results of antenna at location 1.

S. No.	Received signal frequency (MHz)	Received signal power (dBm)	Received signal power (μW)	Received signal (mV) rms
1	958.12	−16.64	21.67	32.91
2	958.28	−16.81	20.8	32.25
3	957.96	−16.82	20.79	32.24
4	957.80	−17.22	18.96	30.78
5	958.44	−17.44	18	30
6	958.60	−19.32	11.69	24.18
7	958.76	−20.92	8	20
8	957.32	−21.61	6.9	18.57
9	958.92	−21.80	6.6	18.16
10	958.12	−16.64	21.67	32.91

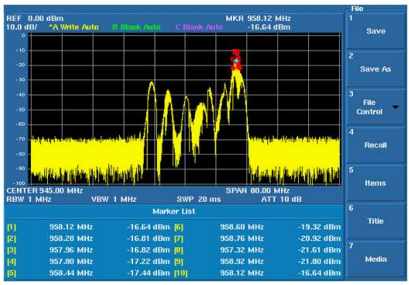

Figure 10. Antenna field test spectrum from GSM-900 cell tower at location 1.

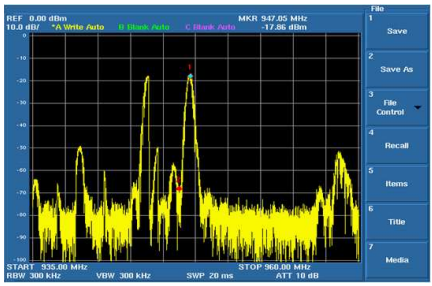

Figure 11. Antenna field test spectrum from GSM-900 cell tower at location 2.

which is close to the measured resonance frequency of antenna which is at 955 MHz with S_{11} of −35 dB. The high power level captured clearly indicates that the 377 Ω impedance of the designed antenna matches closely with the free space impedance 377 Ω.

Location 2: In this location the field test of the receiving E-shaped patch antenna was conducted at the ground level at line of sight with the GSM transmitting antenna located at 50 m above the ground and at a distance of 200 m between them. The power spectrum obtained is shown in Figure 11 and the result of performance is shown in Table 4.

Table 4. Field test results of antenna at location 2.

S. No.	Received signal Frequency (MHz)	Received signal power (dBm)	Received signal power (μW)	Received signal (mV) rms
1	947.10	−17.21	16.36	28.6
2	947.05	−17.86	19	30.82
3	945.85	−21.91	6.44	17.94

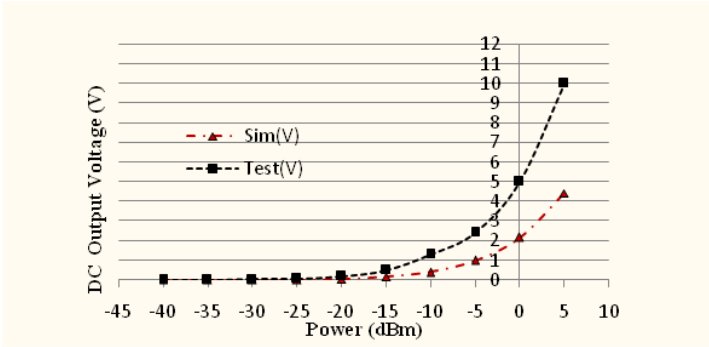

Figure 12. Results of simulation and test for DC output of 7-stage voltage doubler as a function of input power.

It is observed that the antenna capturing signals from 935 MHz to 960 MHz which lies in the downlink radio frequency range of GSM-900 band. The peak signal of −17.86 dBm was observed at 947.05 MHz. The high power level captured clearly shows that the 377 Ω impedance of the antenna matches closely with the free space impedance 377 Ω.

4.3. Results of RF-DC Conversion Module [21]

The simulation and test results of the 7-stage voltage doubler for the DC output voltage is shown in Figure 12.

The analysis shows that the simulated and the measured results have the same trend. The measured results are shown to be better than the simulation results. The reason behind this may be due to the uncertainty in the series resistance value of the diode obtained from SPICE parameters in modeling as explained [21]. This resistance value of the diodes in the practical circuit may be lower than in the model, which provides a faster discharge path that resulted in this increase in

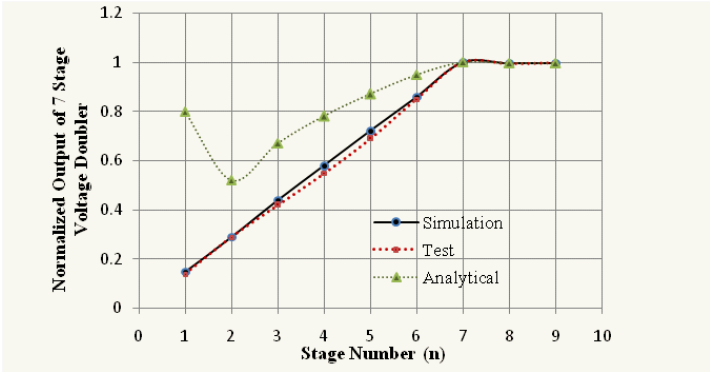

Figure 13. Normalized output of multiplier versus stage number.

voltage as it passes through the stages and reaches to final output. In this work, the DC output voltages obtained through simulation and measurement at 0 dBm are 2.12 V and 5.0 V respectively.

Figure 13 shows the graph for the analytical model of the Equation (6). The output voltage V_0 represents the maximum voltage obtainable for the n-stage multiplier. The simulated and measured voltages recorded at each of the subsequent stages for the 7-stage multiplier also shown in Figure 13. These voltages are nearly the same at all the stages. However, their voltages are less than that obtained from the analytical model until the 7th stage the reason behind this difference is, in the measured and simulated voltages are affected by the presence of the succeeding stages-here the nth stage loads the $n-1$ stage, hence reducing its output voltage.

The doubling effect is seen for all the analytical, simulated and measured results up to 7-stages only, but beyond this there is no increase in the output voltage. For the simulation and measured 9-stages were considered. The result also shows that there is no increase in the output voltage.

4.4. Simulation Results of Pi Matching Network

Figure 14 shows the result of return loss -24.73 dB obtained at resonant frequency (m1) 946.4 MHz. It is observed that the structure resonates at 946.4 MHz and has a bandwidth of 45.8 MHz with the frequency band ranges from 921.9 MHz (m2) to 967.7 MHz (m3), the impedance bandwidth achieved is 4.84% at 946.4 MHz at the centering frequency of the desired band.

The smith chart representation of impedance for pi matching

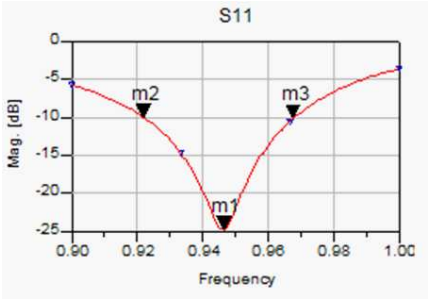

Figure 14. Results of return loss for pi matching network.

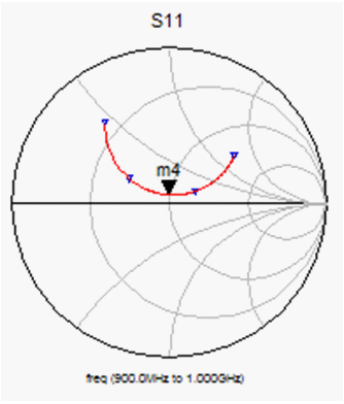

Figure 15. Results of Impedance on Smith chart for pi matching network.

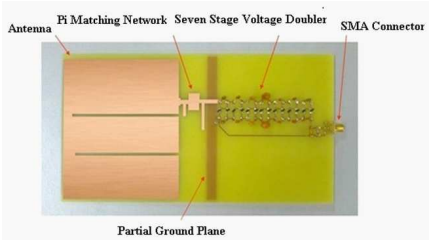

Figure 16. Integrated assembled PCB of RF energy harvesting system for GM-900.

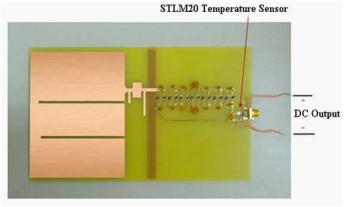

Figure 17. Harvester system connected to the temperature sensor.

network is shown in Figure 15. From the result it is observed that the impedance at 946.4 MHz is equal to $375.87 + j43.73\,\Omega$. From the analysis resistive part of the impedance is very close to impedance of the antenna and reactive part is slightly inductive. This shows that the matching network provides reasonable match for $377\,\Omega$ antenna despite of being slightly inductive.

4.5. Results of RF Energy Harvesting System

The integrated assembly of printed circuit board for the RF energy harvesting system is shown in Figure 16. The harvester system module connected to the application device STLM20 is shown in Figure 17. The overall system was tested using an intentional radio frequency signal source at 900 MHz from a signal generator. The DC output

Table 5. Results of RF energy harvesting system connected to the temperature sensor in the laboratory.

S. No.	Received signal power (dBm)	Received signal power (μW)	Received Signal (mV) rms	DC output voltage obtained (V)	Activation status
1	−21	7.94	19.92	3.84	Activated
2	−22	6.31	17.76	3.63	Activated
3	−23	5.01	15.83	3.34	Activated
4	−24	3.98	14.11	3.12	Activated
5	−25	3.16	12.56	2.82	Activated
6	−26	2.51	11.20	2.61	Activated
7	−27	1.99	9.972	2.14	Deactivated

Table 6. Results of RF energy harvesting system using temperature sensor in the laboratory and in the field.

Test Environment	Analog Output voltage (V)	Temperature (°C) (computed from sensor output voltage of harvesting system)	Temperature (°C) (through thermometer in the lab)	Temperature (°C) (in the PC display using data Acquisition system)
Laboratory	1.592	21	21	21
Field	1.528	30	NA	NA

voltage was used to power the STLM20 temperature sensor. In order for the sensor to function, it requires the voltage source ranging from 2.4 V to 5.4 V at a quiescent supply current of 8.0 μA. Table 5 shows the calculated temperature from Equations (10) and (11). Their results are tabulated against the output voltage of the sensor.

The results show that the temperature recorded using energy harvesting system was the same as measured using the conventional mercury thermometer and also data acquisition system.

A field test was conducted on the harvester system at the ground

level at line of sight with the GSM transmitting antenna in location 2. The DC voltage obtained from the harvester is 2.9 V a distance of 50 m from the tower to power the temperature sensor. The temperature is computed from the output voltage using the Equation (10). The results of the environment temperature using the RF energy harvesting system in the laboratory and field are shown in Table 6. The analysis shows that the environment temperature obtained using the harvester system is accurate for the laboratory and field test.

5. CONCLUSION

A novel 900 MHz RF energy harvesting system for powering low power sensors has been analyzed, discussed, designed, and tested. The novelty lies in the partial ground plane in the antenna structure which resulted in maximizing the energy captured and generating a higher DC output voltage that can power low power devices.

Firstly, a 377 Ω E-shaped patch antenna with partial ground plane with compacted size was designed, simulated and implemented. Compared to the established performance characteristics of wideband micro strip 50 Ω patch antennas, the antenna with the partial ground plane was successes in achieving a wide impedance bandwidth for matching to a free space impedance 377 Ω.

Subsequently the pi matching network located in between antenna and the RF-DC conversion module is designed simulated and implemented to provide a good match from the load to the source.

Lastly the energy conversion module that comprises of 7-stages voltage doubler circuit with zero bias Schottky diodes was successfully designed, implemented, tested and found to be efficient in converting the RF signals captured by the antenna to the required DC output voltage for powering the STLM20 temperature sensor.

ACKNOWLEDGMENT

We would like to acknowledge and thank the Ministry of Higher Education Malaysia for funding this project under the Fundamental Research Grant FRGS/1/10/TK/UNITEN/02/13.

REFERENCES

1. Roundy, S. J., "Energy scavenging for wireless sensor nodes with a focus on vibration to electricity conversion," PhD Thesis, University of California, Berkeley, USA, 2003.

2. Roundy, S., B. Otis, Y. H. Chee, J. Rabaey, and P. Wright, "A 1.9 GHz RF transmit beacon using environmentally scavenged energy," *ACM International Symposium on Low Power Electronics and Design*, 2003.
3. Le, T., K. Mayaram, and T. S. Fiez, "Efficient far-field radio frequency power conversion system for passively powered sensor networks," *IEEE Custom Integrated Circuits Conference (CICC)*, 293–296, Sep. 2006.
4. Sudou, M., H. Takao, K. Sawada, and M. Ishida, "A novel RF induced DC power supply system for integrated ubiquitous micro sensor devices," *International Solid-State Sensors, Actuators and Microsystems Conference*, 907–910, Jun. 2007.
5. Ungan, T. and L. M. Reindl, "Concept for harvesting low ambient RF-sources for microsystems," http://www.imtek.de/content/pdf/public/2007/powermems_2007 paper_ungan.pdf, Accessed on April 9, 2009.
6. Ungan, T. and L. M. Reindl, "Harvesting low ambient RF-sources for autonomous measurement systems," *IEEE Instrumentation and Measurement Technology Conference proceedings*, 62–65, May 2008.
7. Le, T. T., "Efficient power conversion interface circuits for energy harvesting applications," PhD Thesis, Oregon State University, USA, Jun. 2008.
8. Visser, H. J., A. C. F. Reniers, and J. A. C. Theeuwes, "Ambient RF energy scavenging: GSM and WLAN power density measurements," *Proceedings of the 38th European Microwave Conference*, 721–724, Netherlands, Oct. 2008.
9. Asefi, M., S. H. Nasab, L. Albasha, and N. Qaddoumi, "Energizing low power circuits by using an RF signal harvester," *16th Telecommunications Forum TELFOR*, Nov. 2008.
10. Hart, H., K. Lanham, and M. Sass, "S-band radio frequency energy harvesting," Science Applications International Corporation, May 2009.
11. Jabbar, H., Y. S. Song, and T. T. Jeong, "RF energy harvesting system and circuits for charging of mobile devices consumer electrons," *IEEE Transcations on Consumer Electronics*, Vol. 56, No. 1, 247–253, Feb. 2010.
12. Arrawatia, M., M. S. Baghini, and G. Kumar, "RF energy harvesting system at 2.67 and 5.8 GHz," *Proceedings of Asia-Pacific Microwave Conference*, 900–903, 2010.
13. Arrawatia, M., M. S. Baghini, and G. Kumar, "RF energy

harvesting system from cell towers in 900 MHz band," *National Conference on Communications, (NCC) 2011*, 1–5, Jan. 28–30, 2011.

14. http://www.rfwirelesssensors.com/2009/01/intel-ambient-rf-energy-harvesting-demonstration/, Accessed on May 5, 2009.
15. http://www.powercastco.com/PDF/P2110-datasheet.pdf, Accessed on Jun. 14, 2010.
16. Chiam, T. M., L. C. Ong, M. F. Karim, and Y. X. Guo, "5.8 GHz circularly polarized rectennas using schottky diode and LTC5535 rectifier for RF energy harvesting," *2009 Asia-Pacific Microwave Conference (APMC 2009)*, 32–35, 2009.
17. Farinholt, K. M., G. Park, and C. R. Farra, "RF energy transmission for a low-power wireless impedance sensor node," *IEEE Sensors Journal*, Vol. 9, No. 7, 793–800, Jul. 2009.
18. Devi, K. K. A., S. Sadasivam, N. M. Din, C. K. Chakrabarthy, and S. K. Rajib, "Design of a wideband 377 Ω E-shaped patch antenna for RF energy harvesting," *Microwave and Optical Technology Letters*, Vol. 54, No. 3, 569–573, Mar. 2012.
19. Balanis, C. A., *Antenna Theory*, 3rd Edition, John Wiley & Sons, New York, 2005.
20. Stutzman, W. and G. Thiele, *Antenna Theory and Design*, 2nd Edition, ISBN 0-471-02590-9, Wiley, 1997.
21. Devi, K. K. A., N. M. Din, and C. K. Chakrabarthy, "Optimization of the voltage doubler stages in an RF-DC convertor module for energy harvesting," *Circuits and Systems*, Vol. 3, No. 3, Jul. 2012.
22. Harris, D. W., "Wireless battery charging system using radio frequency energy harvesting," Thesis, BS, University of Pittsburgh, Jul. 13–15, 2004.
23. Wong, K. L. and Y. F. Lin, "Small broadband rectangular microstrip antenna with chip-resistor loading," *Electron. Lett.*, Vol. 39, 1593–1594, 1997.
24. STMicroelectronics, "STLM20 application note," http://www.st.com/internet/com/Technical resources/technical literature/application note /CD00174666.pdf, Accessed on Nov. 12, 2010.
25. STMicroelectronics, "STLM20 ultra-low current precision analog temperature sensor," http://www.st.com/, Accessed on Nov. 12, 2010.